Journal of Thermal Analysis and Calorimetry, Vol. 63 (2001) 733–748

THE MECHANISM OF THE THERMAL TRANSFORMATION FROM GOETHITE TO HEMATITE*

D. Walter[1], *G. Buxbaum*[2] *and W. Laqua*[1]

[1]Institut für Anorganische und Analytische Chemie der Justus-Liebig-Universität, Heinrich-Buff-Ring 58, D-35392 Gießen, Germany
[2]Bayer AG, Geschäftsbereich Chemie, Ch-F, D-51368 Leverkusen, Germany

(Received July 17, 2000; in revised form October 30, 2000)

Abstract

Synthetic pigments of goethite (Bayferrox®) of different particle size were investigated by DTA, IR, DSC, TG and X-ray diffraction measurements. It follows that a so-called 'hydrohematite' described in the literature does not exist as a discrete intermediate during the dehydration course from goethite to hematite. Instead we observed a dependence of the dehydration mechanism on the particle size. Transformation enthalpies and activation energies for the dehydration process will be given. A plausible dehydration mechanism, which is compatible with our DTA/DSC results, is deduced from TEM investigations.

Keywords: dehydration, DTA/DSC, goethite, hematite, IR, TEM, TG, XRD

Introduction

Inorganic pigments are of great economical importance because of their chemical stability (i.e. against UV radiation or corrosive gases) and their relatively low production costs. Apart from the white pigment titanium dioxide (TiO_2) there are the iron oxides and hydroxides, which are widespread used. They are contained not only in paints, enamels and varnishes, but they are also main constituents of electromagnetic memory devices because of their unique magnetic properties [1].

All iron oxide and iron hydroxide based pigments are produced from aqueous solutions of water soluble iron salts (nitrates for instance) according to well established industrial processes, named Penniman and Laux process [1] after the inventors of these methods. Individual process parameters like pH, salt concentration, temperature and stirring velocity are of great influence concerning the pigment particle size and geometry, which in turn control the nuances of pigment colours.

The main chemical steps which are of importance during the production of goethite (α-FeOOH) and hematite (α-Fe_2O_3) are well established [2]. On the other

* Dedicated to Prof. Dr. Brigitte Sarry on the occasion of her 80th birthday

1418–2874/2001/ $ 5.00

Akadémiai Kiadó, Budapest
Kluwer Academic Publishers, Dordrecht

hand the mechanism of the solid state transformation from goethite to hematite is not fully understood yet. Wolska *et al*. [3–6] concluded from IR-absorption measurements that the dehydration reaction

$$2\alpha\text{-FeOOH}=\alpha\text{-Fe}_2O_3+H_2O$$

proceeds via a structurally uncharacterised intermediate of the general formula

$$Fe_{2-x}O_{3-3x}(OH)_{3x}\ (x=0:\ \alpha\text{-}Fe_2O_3;\ x=1:\ Fe(OH)_3).$$

This intermediate is referred to as 'hydrohematite' or 'protohematite' in the literature. It is generally assumed that the hydroxyl-groups occupy the O^{2-}-positions within the hematite-structure, forming associates with vacancies in the Fe^{3+}-sublattice [7].

Here we report experimental results which can give some new insight into the mechanism of the goethite to hematite transformation reaction.

Experimental

To investigate the goethite dehydration reaction commercial goethite samples of different particle size (Bayferrox®) were used, produced via the well-known Penniman process [1]. Characteristic data of the samples from REM and BET studies are given in Table 1.

The characteristic needle-shaped habitus of the goethite samples can be seen from REM images given in Fig. 1. The needle surfaces are smooth and neither grooves nor scratches or other artefacts are to be seen. The particle size distribution of the samples is very small [8].

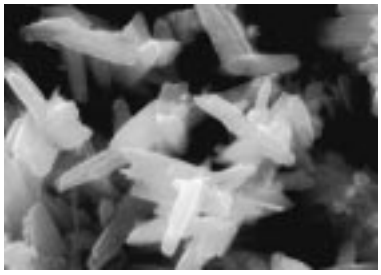

Fig. 1 REM image of goethite 1; magnification: 30 000×

High-temperature XRD measurements (Guinier-method) were performed with $CuK_{\alpha 1}$-radiation, the heating rate was 25°C h^{-1}, using small quartz tubules as sample containers.

DTA-investigations (thermobalance L 81, Linseis, Germany) were carried out with samples in platinum crucibles and heating rates of 5°C min^{-1}. For our DSC measurements we used a Perkin Elmer 7 (sealed gold crucibles, heating rate 20°C min^{-1}). The intricate preparation of goethite needles suitable for TEM investigations is described in the text.

Table 1 Specific surface area of goethite samples (from BET-measurements in nitrogen) and characteristic particle geometry (from SEM images)

Sample	Specific surface/$m^2\ g^{-1}$	Particle geometry/$10^{-18}\ m^3$
Goethite 1	10	1.2×0.25×0.25
Goethite 2	14.5	1.0×0.15×0.15
Goethite 3	67	0.3×0.03×0.03
Goethite 4	149	0.1×0.01×0.01

Results and discussion

High-temperature XRD measurements

The temperature-dependent transformation of goethite-reflexes into hematite-reflexes during the dehydration process was used to determine the relevant transformation temperatures as a function of particle size. Results are given in Table 2.

Table 2 Goethite–hematite transformation temperatures for different particle size, estimated from high-temperature XRD measurements

Sample	*T*/°C
Goethite 1	250.0
Goethite 2	245.8
Goethite 3	237.5
Goethite 4	191.7

Differential thermal analysis

The thermal dehydration process between 200 and 400°C does not change the geometry of the needle-shaped goethite samples, i.e. the newly formed hematite crystals are of the same habitus as the former goethite crystals. Heating the samples to temperatures far beyond the dehydration temperature (T=800°C) results in sintering effects (Fig. 2); firstly needle edges begin to round-off and finally individual crystals start growing together.

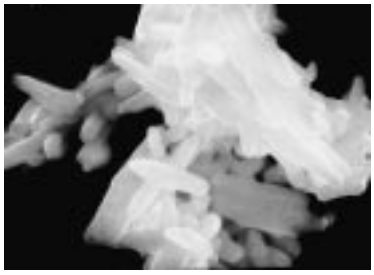

Fig. 2 REM image of goethite 1 after heating to 800°C; magnification 30 000×

Samples with large particle size (goethite 1) lead to DTA curves which show an endothermic double peak [9] at 274.3 and 321.4°C (Fig. 3a). With decreasing particle size the discrete peaks begin to merge (Figs 3b and 3c) and at last a single peak (goethite 4) of nearly ideal shape results at 272.1°C (Fig. 3d), which is characteristic for first order transitions. The temperatures for the peak maxima are arranged in Table 3.

We conclude that in case of small-sized samples the dehydration process is a one-step reaction. A careful analysis of the DTA-results reveals that the area under the dehydration-peak of goethite 4 is smaller in comparison to the more or less split double peak of goethite samples 1–3, which are of larger particle size. This means the reaction enthalpy for the dehydration process from goethite to hematite increases with particle size. An explanation will be given later in this text.

Table 3 Dehydration of goethite: peak-maximum temperatures from DTA measurements

Sample	1. Peak-maximum, *T*/°C	2. Peak-maximum, *T*/°C
Goethite 1	274.3	321.4
Goethite 2	278.1	314.0
Goethite 3	278.1	304.8
Goethite 4	272.1	–

Although the existence of a double peak in the DTA curves (goethite 1–3), even if not completely separated, indicates a two-step mechanism of dehydration, we are not able to determine whether an intermediate product is formed in these cases. Otherwise, the DTA result for goethite 4 clearly indicates a one-step dehydration process. We conclude from the fact that a particle size-dependent mechanism contradicts the existence of a thermodynamically stable discrete intermediate that hydrohematite has not been formed during the dehydration of goethite. Apart from that, as small particles (with large specific surface area) generally show higher chemical reactivity, preferably in the case of goethite 4 the formation of hydrohematite should have been expected, if at all.

Concerning the nature of the observed double-peak a twinning of the goethite needles is discussed in the literature, followed by the assumption that smaller twins dehydrate at lower temperatures [2, 10]. From the following reason we can not accept this argument. According to our DTA results, the first reaction-step (i.e. first peak of the double-peak) indicates a genuine dehydration process, which is independent of particle size (Figs 3a–d). This means, if the discussed assumption of a twin growing mechanism were true, a double-peak in the DTA-plot of goethite 4 should be expected as well. In addition, we could not find any indication in our REM images that a twinning mechanism could play any a role during the dehydration process.

In order to get some insight in the nature of partially dehydrated goethite, we broke off the dehydration runs at temperatures characteristic for the first DTA-peak maximum of goethite 1–3 (Table 2). Afterwards these samples were characterised by IR- and XRD-measurements, as described in the following sections.

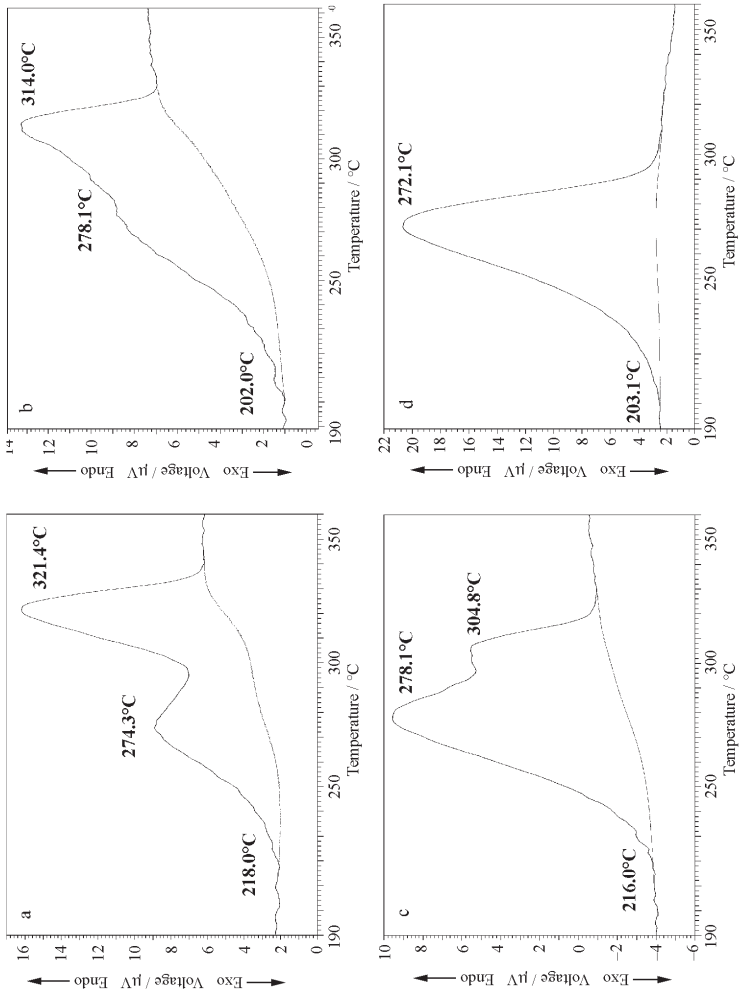

Fig. 3 DTA-plots of a – goethite 1 (10 $m^2 g^{-1}$, heating rate: 5°C min^{-1}); b – goethite 2 (14.5 $m^2 g^{-1}$, heating rate: 5°C min^{-1}); c – goethite 3 (67 $m^2 g^{-1}$, heating rate: 5°C min^{-1}) and d – goethite 4 (149 $m^2 g^{-1}$, heating rate: 5°C min^{-1})

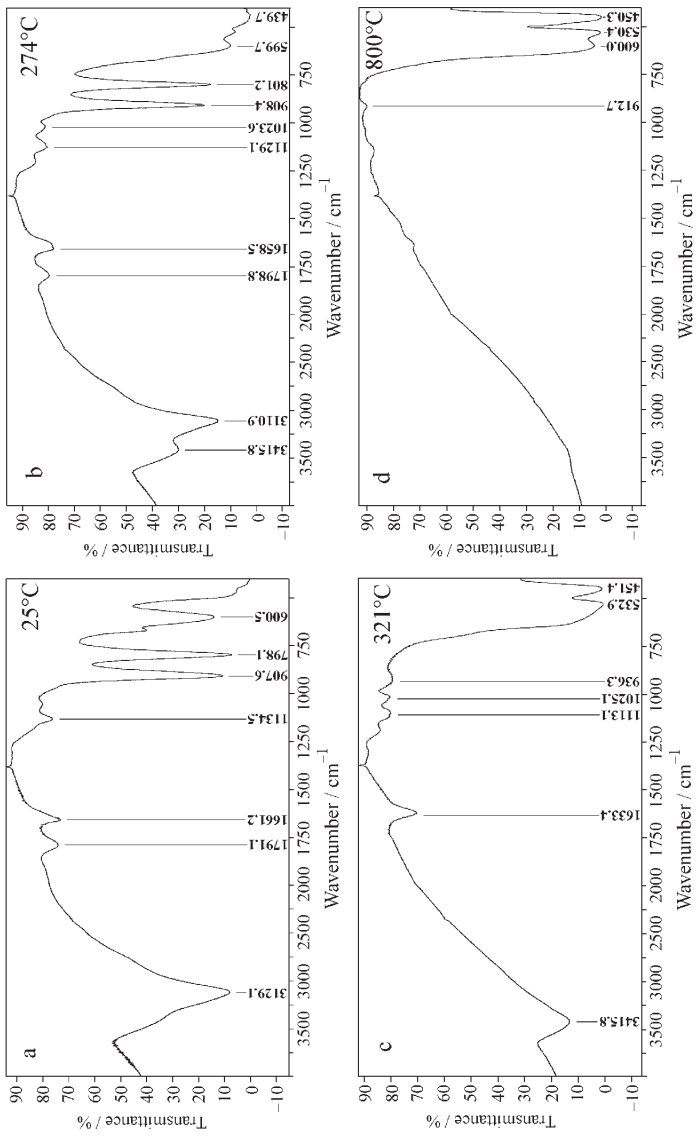

Fig. 4 IR-spectra of a – goethite 1; b – goethite 1 partially dehydrated at 274°C; c – goethite 1 completely dehydrated at 321°C and d – goethite 1 after heating to 800°C, all in the form of KBr-pellets

Infrared spectroscopy

Analogous to Wolska *et al*. [3–6] we measured the IR absorption – using KBr pellets – between 400–4000 cm^{-1}. The IR spectrum of goethite 1 is presented in Fig. 4a. The spectra of the goethite samples 2–4 are not shown, because they show similar characteristics to the spectrum of goethite 1.

The IR spectrum of goethite 1 (Fig. 4a) shows the typical OH-vibration band at ~3129 cm^{-1}. The very weak shoulder near 3415 cm^{-1} is characteristic for surface-adsorbed water. Two smaller bands at 1661 and 1791 cm^{-1} as well as the two bands in the 'fingerprint'-region at 798 and 907 cm^{-1} are caused by the needle-like habitus of the α-FeOOH crystals. The occurrence of specific bands depending on geometrically influenced scattering processes is generally observed in solid-state IR spectra.

The IR spectrum of goethite 1, which was partially dehydrated at 274°C (Fig. 4b) shows no significant change: only the OH-vibration band (now at ~3110 cm^{-1}) is of slightly lower intensity. Goethite 1 completely dehydrated at 321°C (Fig. 4c) has lost its OH-vibration band. However, the H_2O-band at 3415 cm^{-1}, characteristic for surface-adsorbed water, has gained some further intensity [11]. There are no significant bands at 1791 cm^{-1} and in the 'fingerprint'-region. After heating goethite 1 to 800°C (Fig. 4d) all the characteristic bands, seen in the spectrum of goethite 1, have levelled out. This observation is attributed to a continuously progressing sintering process of the needle-shaped crystals (Fig. 2). At the same time, these sintering processes are responsible for the development of some absorption bands in the region <650 cm^{-1}.

From our IR-absorption measurements no support can be deduced for the existence of a distinct intermediate, say hydrohematite.

X-ray diffraction

At room temperature we observed the well-known X-ray pattern for goethite [12]. A decreasing particle size raises the noise level. Completely dehydrated goethite samples (T=400°C) show X-ray patterns typical for hematite.

The X-ray diffraction pattern of partially dehydrated goethite samples 2–3 exhibit both the reflections of goethite and hematite as well; no reflections could be assigned to 'hydrohematite' or any other intermediate [9].

Table 4 Thickness of the hematite layer formed during the dehydration of goethite, after the first dehydration step

Sample	Layer thickness/nm
Goethite 1	30.5
Goethite 2	22.3
Goethite 3	4.9

The intensity decrease of the goethite reflections mirrors at the same time the amount of hematite formed during the dehydration process. We estimated this hema-

tite amount from the intensity ratio between the (110) reflection of partially dehydrated samples 1–3 and the respective non-treated samples. With a precise knowledge of the needle geometry and based on the assumption that the dehydration front moves from the outer needle surface to the needle centre, we were able to calculate the particle size dependence of the hematite layer thickness (Table 4) [13].

Differential scanning calorimetry

To estimate the enthalpies for the transformation of goethite into hematite, we performed DSC measurements. A typical result is shown in Fig. 5. Perkin Elmer 7 Series thermal analysis system was used.

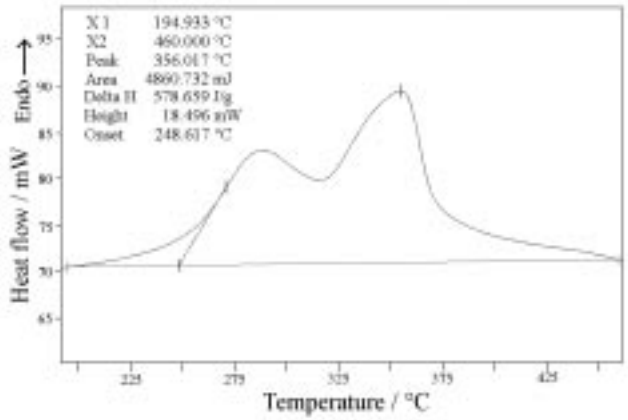

Fig. 5 DSC-plot of goethite 1, sample mass 8.400 mg, heating rate: 20°C min^{-1}

Taking into account our results on the degree of transformation of partially dehydrated goethite into hematite after passing the first dehydration step, we were able to calculate the transformation enthalpies given in Table 5.

Table 5 Enthalpies for the transformation of goethite and partially dehydrated goethite into hematite as a function of particle size

Sample	Enthalpy/kJ mol^{-1}
Goethite 1	51.43
Goethite 1 (partially dehydrated)	29.49
Goethite 2	41.30
Goethite 2 (partially dehydrated)	26.56
Goethite 3	31.62
Goethite 3 (partially dehydrated)	19.81
Goethite 4	25.85

It is clearly to be seen that the transformation enthalpies increase with particle size.

Thermogravimetry

Experiments with constant heating rates

From the TG curves for goethite samples 1–3, given in Fig. 6, we conclude that the mass decrease can exclusively be attributed to a loss of water. Apart from that it is evident that the dehydration proceeds via a two-step mechanism, whereby the completion of the first dehydration step is indicated by the turning point of the dehydration plots. No such turning point can be found in the dehydration plot of goethite 4, supporting our assumption that the dehydration of goethite 4 is a one-step reaction. These results are consistent with our results from DTA measurements.

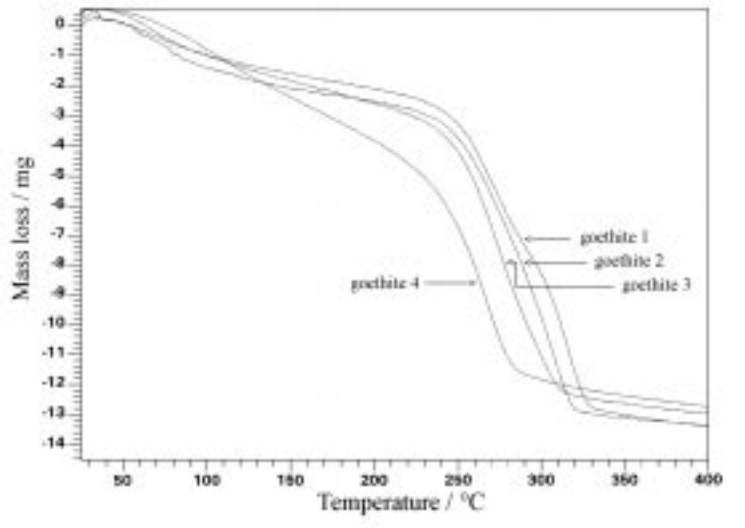

Fig. 6 TG for goethite samples of different particle size, heating rate: 5°C min^{-1}

The small mass decrease up to temperatures of about 150°C can be explained by a loss of surface-adsorbed water; it follows that, the smaller the particle size the stronger the water molecules are bound to the surface.

Experiments under isothermal conditions

To get information on the kinetics of the dehydration process we performed isothermal TG investigations (corundum crucible, mass content: 150 mg). The samples were heated with 5°C min^{-1} to a temperature 20°C below the temperature, where the isothermal dehydration starts. From there on the heating rate was lowered to 1°C min^{-1} until the desired temperature was reached. Complete dehydration at this temperature took place within a maximum of 300 min at the lowest dehydration temperature. To obtain insight in whether the second dehydration step is kinetically controlled or not, we additionally followed the dehydration at 274°C in case of goethite 1. Results are presented in Figs 7 a–d.

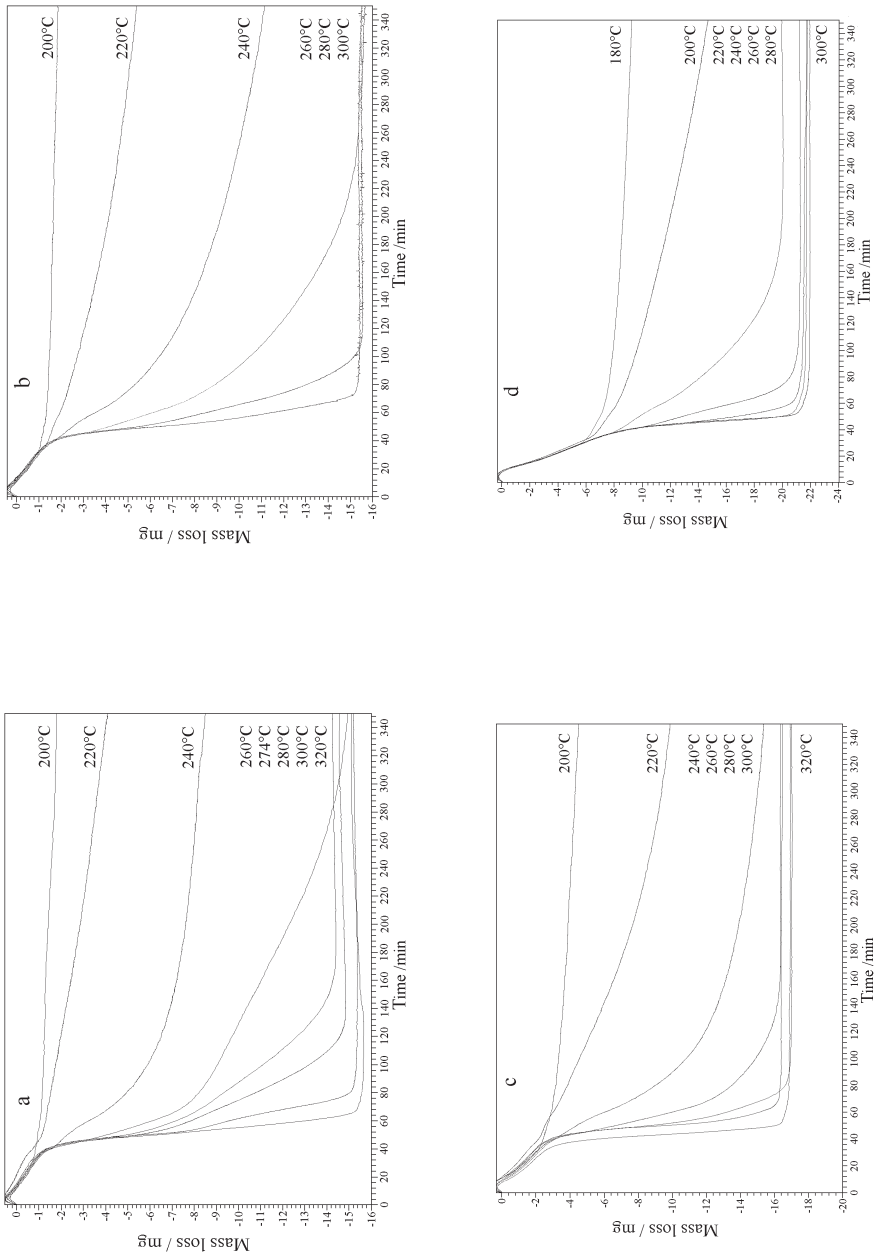

Fig. 7 Time dependent isothermal mass change of goethite samples a – goethite 1, b – goethite 2, c – goethite 3, d – goethite 4

The mass decrease during the induction period (about 50 min) results from loss of surface water. No further mass change occurs as long as the temperatures are below the dehydration temperature, which lies about 20°C below the maximum temperature of the corresponding DTA peak. The insignificant mass loss within the temperature range, where no dehydration takes place, can be attributed to the release of very small residual surface water. At temperatures 20°C below the DTA peak maximum, the dehydration proceeds continuously over a period of several hours. Above 274°C shorter reaction times are sufficient for completion of the dehydration process.

The reaction rate constants k for the dehydration process were estimated according to the so-called shrinking-core model, which reads for crystallites with cylindrical geometry [14–17]:

$$1-(1-\alpha)^{1/2} = k\frac{V_m t}{r}$$

where α=degree of transformation, V_m=molar volume of goethite, r=particle radius, t=time.

The activation energies, which we calculated from the corresponding Arrhenius plot, can be found in Table 6.

Table 6 Particle size dependence of the activation energy for the goethite dehydration

Sample	Particle radius/nm	Surface area/$m^2\ g^{-1}$	Activation energy/kJ mol^{-1}
Goethite 1	125	10	114.3
Goethite 2	75	14.5	137.8
Goethite 3	15	67	113.5
Goethite 4	5	149	107.4

Because we have not been able to separate reaction steps 1 and 2 during our TG experiments, the activation energies given in Table 6 describe the overall dehydration reaction including both the reaction steps 1 and 2.

The particle size dependence of the activation energy seems to be negligible. Our results are in good agreement with values given by Pelino *et al.* [14], who found 119 kJ mol^{-1} for samples with a specific surface area of 14.1 $m^2\ g^{-1}$.

TEM experiments

Further support for our dehydration model comes from TEM results of partially dehydrated goethite samples. We investigated needle areas oriented nearly parallel as well as strictly perpendicular to the needle axis.

The preparation of such special orientations is a very time consuming and laborious process. A very great number of experiments was necessary to succeed at last. The main aspects of the preparation procedure will be given here, details can be found elsewhere [18]. Small amounts of goethite were immersed into a freshly prepared mixture of polyvinylchloride and a so-called master batch. After the polymeri-

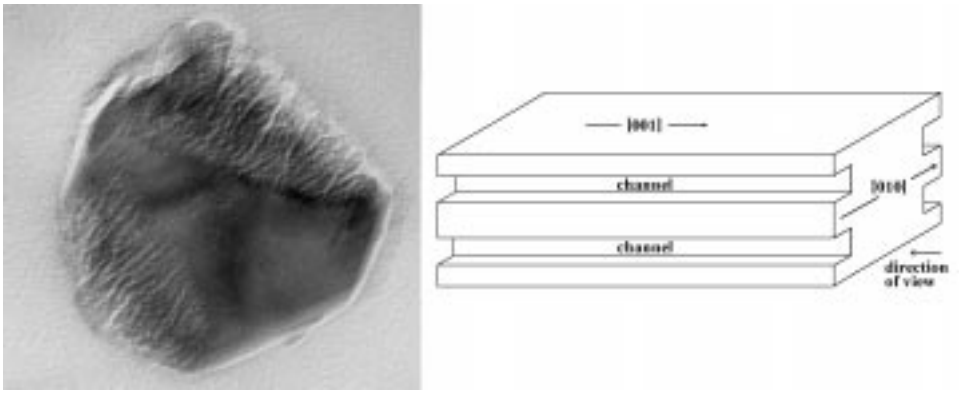

Fig. 8 TEM-image of a partly dehydrated goethite needle cut perpendicular to the needle axis; magnification 225 000×

sation process was finished, the resulting composite was hot-rolled at 70°C, whereby the needles became oriented in such a way that their long axis was aligned parallel to the rolling direction. Suitable parts of such a polymer foil were than fixed in an ultra microtome (Leica Reichert Ultracut S) and cut. These cuttings were useful for TEM investigations perpendicular to the crystallographic *c*-axis. It can be seen from Fig. 8, which shows an example that the needle cross section is neither rectangular [19] nor circular [14] but polygonal instead.

Apart from that we were able to find also needle fragments within the same polymer matrix, which were accidentally crushed by the cutting edge of the microtome in such a way that the fragmented area was aligned nearly parallel to the crystallographic *c*-axis. An example is given in Fig. 9.

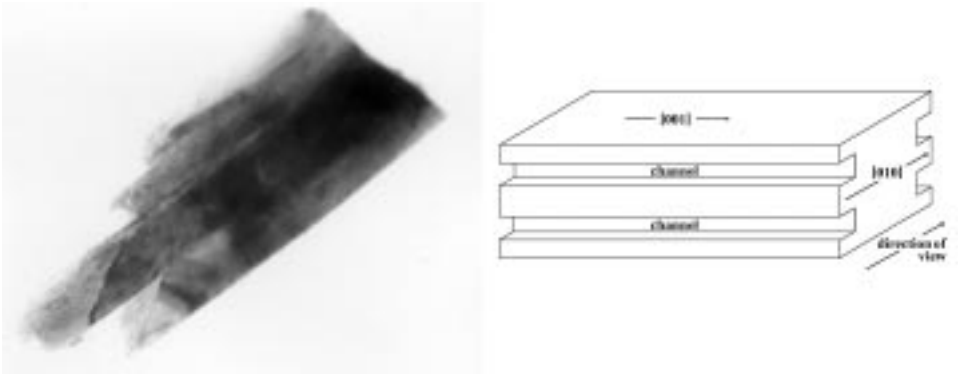

Fig. 9 TEM-image of a fragment of partially dehydrated goethite; magnification 100 000×

To our knowledge this is the first time that it is possible to present TEM images of a partially dehydrated goethite needles cut perpendicular to the needle axis.

Pore-like linear channels oriented parallel to the needle axis are to be seen with regular spacings of about 20 nm between them. (Figure 9, left-hand part of the fragmented needle.) Similar channels were observed by Giovanoli and Brütsch [20] as well as by Hirikawa *et al*. [21] by TEM. Watari *et al*. [22–24] found by electron diffraction that the matrix between the individual channels consists of hematite.

It is worth mentioning that during the dehydration of diaspore (α-AlOOH) within a TEM similar channels were found to be formed [25]. The matrix between the channels consists of corundum (α-Al_2O_3).

Between 325 and 400°C the channels begin to grow together forming oval-shaped pores; above ~650°C pores do not exist any longer [26].

Looking at Fig. 8, which shows the TEM image of a needle-cross section, partially dehydrated at 274°C, we observe that the channels described in the foregoing paragraph have penetrated the needle, starting from two opposite (010)-faces only partly, whereas within the needle centre no dehydration has yet taken place. In addition, it can be seen from Fig. 8 that within the outer parts of the dehydrated areas the channels have vanished and a dense hematite layer has been formed. It is this dense hematite layer which impedes the water molecules from leaving the crystal lattice and explains the extra enthalpy we found in our DTA experiments.

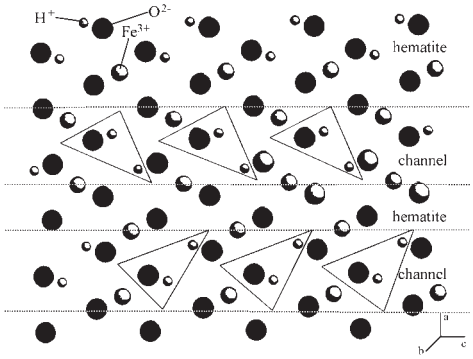

Fig. 10 Excerpt of the goethite crystal structure. The water molecules formed by dehydration are marked by triangles

Keeping the crystal structure of goethite in mind (Fig. 10), a simple model concerning the dehydration mechanism of needle-like goethite becomes plausible. In Fig. 10 we have enclosed every two H-atoms and the next-nearest O-atom with a triangle, thus emphasising that the quasi pre-formed water molecules are arranged in a line parallel to the crystallographic *c*-axis. Between these arrays, which are predisposed to form water molecules, H-free areas containing only iron- and oxygen ions pre-determined to form hematite can be found. Because the diffusion distance for the water molecules to leave the goethite needle along the *c*-axis is too great, they instead escape perpendicular to the *c*-axis in the [010] direction.

This explains the observation that a marked formation of hematite is only to be seen at to opposite surfaces of a goethite needle ((010)-crystal face), with only minor hematite formation at the other opposite surfaces, namely the (001)-crystal faces.

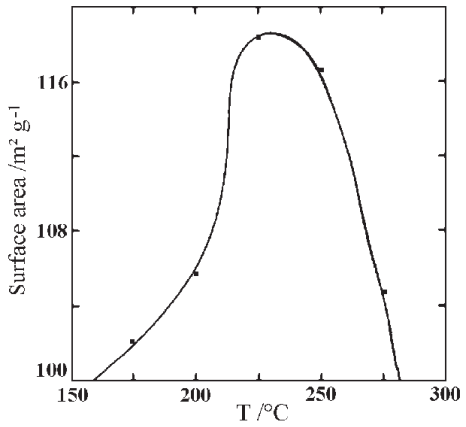

Fig. 11 Variation of the specific surface area of a goethite sample in dependence on the temperature (specific surface area: 14 m^2 g^{-1}) [14]

According to Pelino *et al*. [14] the specific surface area (BET) of goethite passes through a maximum while the dehydration with increasing temperature is in progress (Fig. 11).

The temperature of the maximum corresponds to the complete dehydration of the sample. At this point the number of dehydration channels reaches a maximum as well. At higher temperatures the channels merge and form larger macro pores, which diminish the specific needle surface area.

This explains why goethite 1, totally dehydrated at 321°C, strongly adsorbs water at the surface and gives rise to the OH-vibration band which we found in the IR-spectrum of the total dehydrated goethite at 321°C (Fig. 4c).

Conclusions

From our experimental results we could not get any hint that hydrohematite, postulated in the literature [3–6], does form during the dehydration of goethite. We found that hematite is the only reaction product, which forms in the course of the dehydration process.

Based on the assumption that the thermal dehydration proceeds from the crystal surface to the centre of the goethite needles we developed the following model for the mechanism of the dehydration process: at an early stage of the dehydration, water leaves the crystal lattice in the [010] direction of the crystal by developing dehydration channels parallel to the crystallographic c-axis [001]. The matrix between the channels is formed by hematite.

In case of greater crystal dimensions the dehydration channels within the outer crystal regions begin to grow together, forming a compact hematite layer at the crystal surface, whereas the dehydration front within the needle has not reached the crystal centre, i.e. the dehydration process is not finished yet.

The compact surface hematite layer acts like a barrier, which hampers the further extension of the dehydration zone, because an additional amount of enthalpy must be provided to overcome the dehydration barrier and thus allow the dehydration front to proceed into the needle centre, until the dehydration has finished. Experimental evidence for this model consists of the second peak in the DTA plots of goethite samples 1–3 (Fig. 3).

In case of very small needle dimensions (goethite sample 4) the dehydration is finished before the surface hematite layer reaches a 'critical' thickness, thus a dehydration barrier can not form. The thickness of the critical hematite layer postulated here increases with the size of the goethite needles.

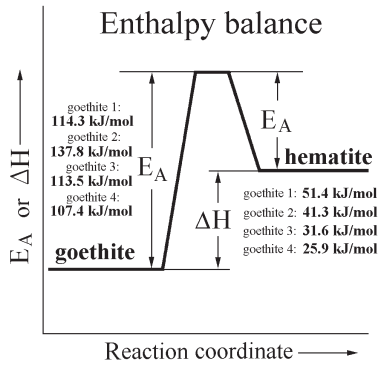

Fig. 12 Graphic representation of the enthalpy changes during the goethite dehydration according to our experimental results

A schematic representation of our experimental results concerning the enthalpy change for the individual dehydration steps is given in Fig. 12.

* * *

We are indebted to Professor H. Lutz (Siegen) and Professor W. Mader (Bonn) for helpful discussions of our IR- and TEM results.

References

1 G. Buxbaum and H. Printzen, Ullmann´s Encyclopedia of Industrial Chemistry, Vol. A20 (1992) 297.
2 R. M. Cornell and U. Schwertmann, The Iron Oxides, VCH-Weinheim, New York, Basel, Cambridge, Tokyo 1996.
3 E. Wolska, Z. Kristallogr., 154 (1981) 69.
4 E. Wolska and W. Szajda, J. Mat. Science, 20 (1985) 4407.

5 E. Wolska, Sol. State Ionics, 28–30 (1988) 1349.
6 E. Wolska and U. Schwertmann, Z. Kristallogr., 189 (1989) 223.
7 G. F. Hüttig and E. Strotzer, Z. Anorg. Allg. Chem., 226 (1936) 97.
8 H. G. Völz and G. Weber, Farbe und Lack, 8 (1984) 642.
9 R. Derie, M. Ghodsi and C. Calvo-Roche, J. Thermal Anal., 9 (1976) 435.
10 U. Schwertmann and R. M. Cornell, Iron Oxides in the Laboratory, VCH-Weinheim, New York, 1991.
11 C. H. Rochester and S. A. Topham, J. Chem. Soc. Faraday Trans. I, 75 (1979) 1073.
12 J. L. Rendon, P. Cornejo, P. de Arambarri and C. J. Serna, J. Colloid and Interface Science, 92 (1983) 509.
13 D. Walter and W. Laqua, Festkörperchemie als Grundlage der Materialforschung, 7. Vortragstagung der GDCh Bonn, 1994.
14 M. Pelino, L. Toro, M. Petroni, A. Florindi and C. Cantalini, J. Mat. Science, 24 (1989) 409.
15 J. Lima de Faria, Z. Kristallogr., 119 (1963) 176.
16 M. C. Ball and H. F. Taylor, Miner. Mag., 32 (1961) 754.
17 O. Levenspiel, Ingegneria delle reazioni chimiche, Ed. Ambrosiana, Mailand 1978.
18 D. Walter, Dissertation, Justus-Liebig-Universität Gießen, 1996.
19 R. M. Cornell, A. M. Posner and J. P. Quirk, J. Inorg. Nucl. Chem., 36 (1974) 1937.
20 R. Givanoli and R. Brütsch, Thermochim. Acta, 13 (1975) 15.
21 S. Hirokawa, T. Naito and T. Yamaguchi, J. Colloid and Interface Science, 112 (1986) 268.
22 F. Watari, J. van Landuyt, P. Delavignette and S. Amelinckx, J. Solid State Chem., 29 (1979) 137.
23 F. Watari, J. van Landuyt, P. Delavignette and S. Amelinckx, J. Solid State Chem., 29 (1979) 417.
24 F. Watari, J. van Landuyt, P. Delavignette and S. Amelinckx, J. Solid State Chem., 48 (1983) 49.
25 B. Zimmermann and W. Mader, Phasenumwandlungen und Reaktionen in Festkörpern, 8. Vortragstagung der GDCh, Darmstadt 1996.
26 M. P. Pomies, M. Menu and C. Vignaud, J. European Ceramic Soc., 19 (1999) 1605.
27 C. J. Goss, Mineral. Magazine, 51 (1987) 437.
28 L. Diamandescu, D. Mihaila-Tarabasanu and M. Feder, Mat. Letters, 17 (1993) 309.